INTERNATIONAL JOURNAL FOR NUMERICAL METHODS IN FLUIDS
Int. J. Numer. Meth. Fluids 2003; **41**:653–673 (DOI: 10.1002/fld.465)

PDF of distance function for level-set flamelet library modelling

P. Nilsson[†] and X. S. Bai[*,‡]

Division of Fluid Mechanics, Lund Institute of Technology, Lund S-221 00, Sweden

SUMMARY

The difference between a presumed distribution of flamelet position and a numerically simulated distribution of distance function (a signed distance to flamelet) is investigated. It is shown that even if the distribution of flamelet position is symmetrical and close to Gaussian, the distribution of distance function away from the mean flame position is skewed towards the mean position and the mean of the distance function is also different from the distance to the mean position. The difference depends on the distance to the mean flame and the flame wrinkling amplitude. An extension method for the variance of the distance function and an upwind scheme for solving the re-initialization equation are presented. A numerical simulation of a premixed turbulent flame is compared to experimental data. Copyright © 2003 John Wiley & Sons, Ltd.

KEY WORDS: level-set; distance function; re-initialization; flamelet; PDF

1. INTRODUCTION

Level-set methods are often used in the modelling of premixed turbulent combustion with flamelet libraries. The reason is that in premixed flames there is no conserved scalar, such as the mixture fraction in non-premixed flames, to calculate the instantaneous or mean flame position. Instead, the instantaneous flame front is often represented by the iso-surface $G = 0$ of a scalar G. The level-set equation for G can be derived from the kinematic balance between the gas flow velocity and the burning velocity of the mixture relative to the gas [1]. Similarly, the mean flame front can be represented by the iso-surface $\tilde{G} = 0$. The equation for the mean level-set function ($\tilde{G}$) can be obtained through the balance between the mean flow velocity and the mean turbulent burning speed.

* Correspondence to: Xue-Song Bai, Division of Fluid Mechanics, Lund Institute of Technology, LTH, Box 118, SE-221-00 Lund, Sweden.
† Current address: ÅF-Processdesign AB, P.O. Box 22226, Helsingborg 250 24, Sweden.
‡ E-mail: bai@mail.vok.lth.se

Contract/grant sponsor: Swedish National Energy Administration's Consortium for Gas Turbine Centre (GTC)
Contract/grant sponsor: Swedish Research Council (VR)

Received February 2002
Revised 16 October 2002

In direct numerical simulations (DNS) the instantaneous flame surface position can be calculated, but in averaged approaches a mean flame surface is traced instead. In Reynolds-, or Favre-averaged Navier Stokes (RANS) equation based approaches, such as a modelling in the $k-\varepsilon$ frame-work, it is not sufficient to use the $\tilde{G}=0$ level surface. A probability density function (PDF) of flamelet position is also needed to describe the turbulent flame brush. To describe the flowfield outside the mean flame brush, information about the distance to the flamelet is needed, for which, a new quantity—a distance function, is introduced. The distance function is defined as the signed distance to the instantaneous laminar flamelet in turbulent flames. The position of the flamelet may be defined at the inner-layer of the chemical reaction zone, at which the production rate of radicals is equal to the consumption rate of radicals. The absolute value of a distance function at a given flowfield point is equal to the distance from the point to the flamelet. The sign of the distance function denotes the relative position of the point to flamelet: a positive distance function indicates the studied flowfield point locates at the burned postflame region, while a negative one corresponds to the unburned region. The mean distance function which is the averaged signed distance to the flamelet surface, is employed in ensemble averaging of the flamelet library over a presumed probability distribution of distance function. Mean density, temperature, viscosity and species concentrations at any point in the flowfield can be calculated using the ensemble average [2–4]. The solution for mean density and viscosity are coupled with the numerical solution of the RANS equations in an iterative procedure.

There is a difference between the distribution of flamelet position and the distribution of distance function. The latter should be employed in the ensemble averaging. This difference is investigated in the present work. An ensemble of different flame shapes is generated and statistics is calculated so that the actual distributions of flamelet position and distance function can be compared.

In order to compute the probability distributions with sufficient accuracy, care has to be taken in the re-initialization. The re-initialization is the process in which the distance function is computed in all points of the domain outside the flame surface. It is essential to maintain an upwinding discretization at the flame surface in order not to disturb this surface in the re-initialization. Therefore the sub-cell fix scheme [5], modified for non-isotropic grids, is presented here.

A solution method for information extension is also presented here. It is shown that the variance of the distribution of distance function may be modelled as constant along a normal to the mean flame surface. In order to perform the ensemble averaging of libraries over distributions, the variance of the probability distribution has to be known in addition to the mean value and the presumed PDF shape. The variance depends on the fluctuations of flame position around the mean flame surface ($\tilde{G}=0$). Therefore the variance at $\tilde{G}=0$ has to be computed first. An extension method is then necessary to extend this information to all points in the domain.

This paper begins with a short review of the RANS level-set flamelet library approach (FLA) for premixed turbulent combustion, followed by a description of the extension methods. Thereafter a description of the re-initialization procedure is presented. The main focus, the difference between the probability distribution of distance function and the distribution of flamelet position is then investigated. The methods are also applied to the simulation of a lean premixed turbulent flame and the results are compared to experimental data.

2. LEVEL-SET FLA

2.1. G-field

In the FLA, the mean position of a turbulent flame front is described with the $\bar{G}$-equation:

$$\dot{\bar{G}} + \tilde{\mathbf{u}} \cdot \nabla \bar{G} = s_T |\nabla \bar{G}| \quad \text{for } \bar{G} = 0 \tag{1}$$

The $\bar{G}$-equation is only used to determine the mean flame position, i.e. the $\bar{G} = 0$ surface. The Favre averaged fluid velocity is denoted with $\tilde{\mathbf{u}}$ and the flame surface propagates relative to the fluid with the speed s_T in a direction normal to the surface. The mean flame propagation speed, which is also referred to as the turbulent burning velocity, is only defined at the mean flame surface, i.e. at $\bar{G} = 0$. $\bar{G}$ is a mean distance function after solving the following equation

$$|\nabla \bar{G}| = \sigma \quad \text{for } \bar{G} \neq 0 \tag{2}$$

σ is a positive variable. It is unity far outside the mean flame brush and $\sigma \ll 1$ near the mean flame position. This parameter will be further discussed below. Equation (2) determines $\bar{G}$ outside the $\bar{G} = 0$ surface and only the position of the $\bar{G} = 0$ surface is determined by Equation (1). The solution of Equation (2) after the solution of Equation (1) is referred to as re-initialization or re-normalization.

If $\bar{G}$ and $\tilde{\mathbf{u}}$ are replaced by their corresponding instantaneous variables, and s_T replaced by the local laminar burning velocity, Equation (1) describes the instantaneous flamelet position in the turbulent flowfield. If $\bar{G}$ is replaced by G and σ replaced by unity, G from Equation (2) is the instantaneous distance function. In Sections 4 and 5, this set of equations for instantaneous G is used to study the PDF distribution of the flamelet position and distance function.

2.2. Ensemble averaging

The average molar fractions, temperature and density, at any given point (x, y, z) of the flow field, are obtained with an integration over the flamelet library, $X(g)$ times the PDF of distance function, $\wp(g)$.

$$\bar{X} = \int_{-\infty}^{\infty} X(g) \wp(g) \, \mathrm{d}g \tag{3}$$

Here g is an integration variable in the sample space of distance function. The flamelet library ($X(g)$) contains the distribution profiles of density, temperature, viscosity and species concentrations across the laminar flamelet (as a function of distance function) [3, 4]. In order to perform the above integration, the PDF of distance function ($\wp(g)$), which is related to the PDF of the flamelet position, has to be known.

As a first approximation, the shape of the PDF of distance function can be assumed to be similar to that of the PDF of flamelet position. The variance of the PDF may be approximately constant along a normal to the mean flame surface. This assumption is more accurate for a one-dimensional turbulent flame. However, For two or three-dimensional flames it is less justifiable (see Figure 1). This issue will be explored in Section 5. The distribution of flame position around the mean flame surface is often assumed Gaussian, as indicated from experiments [6, 7].

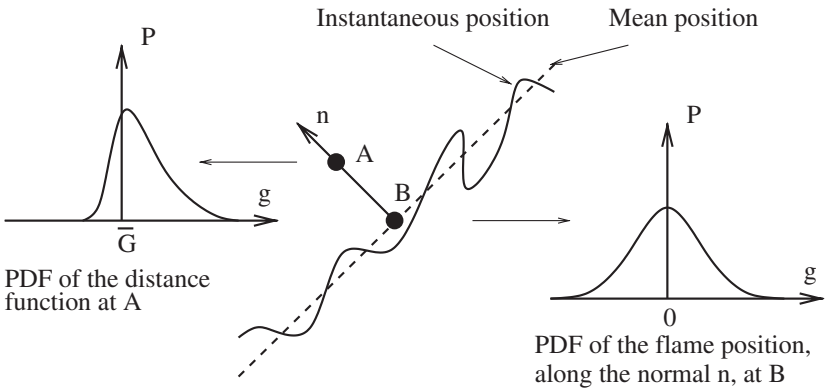

Figure 1. Sketch of PDFs of distance function and flamelet position.

3. EXTENSION METHODS

Several quantities such as the turbulent burning speed and variance of flamelet position, are only defined at the mean flame position. These quantities can be extended outside the mean flame brush.

3.1. Velocity extension

In order to solve Equations (1) and (2) simultaneously, term $s_T\sigma - \tilde{\mathbf{u}} \cdot \nabla \bar{G}$ can be redefined and computed with an extension method, so that all levels along the normal of the $\bar{G} = 0$ level surface propagates with the same velocity. Then the distance function will automatically persist when the $\bar{G} = 0$ surface moves.

3.2. Scalar extension

If a scalar f (e.g. the variance of G) is constant along the normal of the $\bar{G} = 0$ surface, the projection of the gradient of f on the direction normal to the $\bar{G} = 0$ surface is zero:

$$\nabla \bar{G} \cdot \nabla f = 0 \tag{4}$$

which, in two-dimensional form, can be written and discretized on a Cartesian grid as

$$\frac{\partial \bar{G}}{\partial x}\frac{\partial f}{\partial x} + \frac{\partial \bar{G}}{\partial z}\frac{\partial f}{\partial z} = 0 \Rightarrow \underbrace{\frac{\Delta_x \bar{G}}{\Delta x \Delta x}}_{\delta_x} \Delta_x^{\text{up}} f + \underbrace{\frac{\Delta_z \bar{G}}{\Delta z \Delta z}}_{\delta_z} \Delta_z^{\text{up}} f = 0 \tag{5}$$

The derivatives of $\bar{G}$ can be estimated with a central difference here and are denoted with $\Delta_x \bar{G}/\Delta x$ and $\Delta_z \bar{G}/\Delta z$, respectively. The scalar f has to be computed with an upwind difference, depending on which two neighbours have the lowest absolute values of $\bar{G}$, i.e. f-information should propagate from the flame position, $\bar{G} = 0$. The derivatives of f are denoted with $\Delta_x^{\text{up}} f/\Delta x$ and $\Delta_z^{\text{up}} f/\Delta z$, respectively. The upwinding is only necessary for the scalar f, since the $\bar{G}$ field is not updated here.

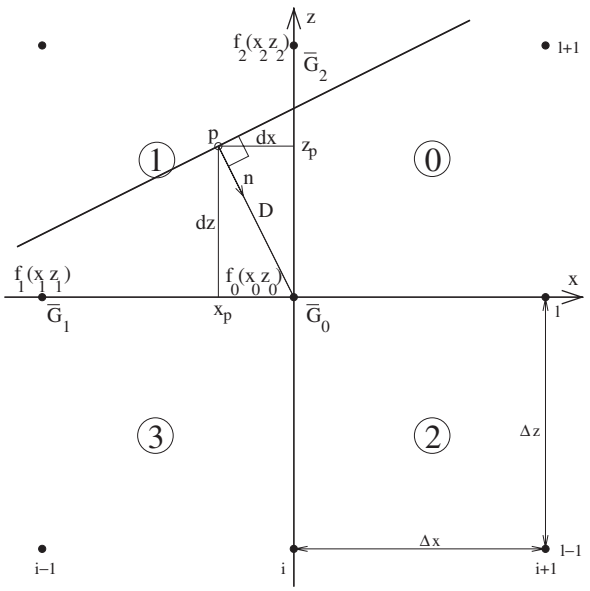

Figure 2. Extension in quadrant $Q = 1$.

To determine from which direction f-information should come, i.e. where the $\bar{G} = 0$ surface is, a quadrant notation (Q) is employed. It is built from two binary switches, Q_x and Q_z:

$$
\begin{aligned}
Q_x &= \begin{cases} 1 & |\bar{G}_{i-1,l}| < |\bar{G}_{i+1,l}| \\ 0 & \text{else} \end{cases} \\
Q_z &= \begin{cases} 2 & |\bar{G}_{i,l-1}| < |\bar{G}_{i,l+1}| \\ 0 & \text{else} \end{cases} \\
Q &= Q_x + Q_z
\end{aligned}
\tag{6}
$$

The four quadrants (Q) can be seen in Figure 2.

If the $\bar{G} = 0$ surface is between the point i, l and one of its closest neighbours, it is called a *close* point. Otherwise it is called a *far* point. A switch is designed to check whether a point i, l is close or far:

$$
\begin{aligned}
&\text{close} \quad \begin{cases} \bar{G}_{i,l}\bar{G}_{i-1,l} < 0 \\ \bar{G}_{i,l}\bar{G}_{i+1,l} < 0 \\ \bar{G}_{i,l}\bar{G}_{i,l-1} < 0 \\ \bar{G}_{i,l}\bar{G}_{i,l+1} < 0 \end{cases} \\
&\text{far} \qquad \text{else}
\end{aligned}
\tag{7}
$$

3.3. Far points

In far points, f can be extended by the following four expressions for the quadrants, respectively:

$\mathbf{Q}=0$:

$$\begin{aligned}
&\delta_x(f_{i+1,l}-f_{i,l})+\delta_z(f_{i,l+1}-f_{i,l})=0\\
&\Rightarrow -f_{i,l}\underbrace{(\delta_x+\delta_z)}_{\delta_+}+f_{i+1,l}\delta_x+f_{i,l+1}\delta_z=0\\
&\Rightarrow f_{i,l}=\frac{1}{\delta_+}(f_{i+1,l}\delta_x+f_{i,l+1}\delta_z)
\end{aligned}\tag{8}$$

$\mathbf{Q}=1$:

$$\begin{aligned}
&\delta_x(f_{i,l}-f_{i-1,l})+\delta_z(f_{i,l+1}-f_{i,l})=0\\
&\Rightarrow f_{i,l}\underbrace{(\delta_x-\delta_z)}_{\delta_-}-f_{i-1,l}\delta_x+f_{i,l+1}\delta_z=0\\
&\Rightarrow f_{i,l}=\frac{1}{\delta_-}(f_{i-1,l}\delta_x-f_{i,l+1}\delta_z)
\end{aligned}\tag{9}$$

$\mathbf{Q}=2$:

$$\begin{aligned}
&\delta_x(f_{i+1,l}-f_{i,l})+\delta_z(f_{i,l}-f_{i,l-1})=0\\
&\Rightarrow -f_{i,l}\underbrace{(\delta_x-\delta_z)}_{\delta_-}+f_{i+1,l}\delta_x-f_{i,l-1}\delta_z=0\\
&\Rightarrow f_{i,l}=\frac{1}{\delta_-}(f_{i+1,l}\delta_x-f_{i,l-1}\delta_z)
\end{aligned}\tag{10}$$

$\mathbf{Q}=3$:

$$\begin{aligned}
&\delta_x(f_{i,l}-f_{i-1,l})+\delta_z(f_{i,l}-f_{i,l-1})=0\\
&\Rightarrow f_{i,l}\underbrace{(\delta_x+\delta_z)}_{\delta_+}-f_{i-1,l}\delta_x-f_{i,l-1}\delta_z=0\\
&\Rightarrow f_{i,l}=\frac{1}{\delta_+}(f_{i+1,l}\delta_x+f_{i,l+1}\delta_z)
\end{aligned}\tag{11}$$

3.4. Close points

For the case of the $\bar{G}=0$ surface being close, a modification is necessary, because here f at the actual surface $\bar{G}=0$ has to be estimated. This is done in the following way. If the $\bar{G}=0$ surface is located as in Figure 2, f in the updated point, (x_0, z_0), should be taken from the point p. The co-ordinates of point p are computed by

$$\begin{aligned}(x_p, z_p) &= (x_0 - \mathrm{d}x, z_0 + \mathrm{d}z)\\ \mathrm{d}x = \bar{G}_0 \frac{\Delta_x \bar{G}_0}{\Delta x}, &\quad \mathrm{d}z = \bar{G}_0 \frac{\Delta_z \bar{G}_0}{\Delta z}\end{aligned} \tag{12}$$

The value of f in point p, f_p, is estimated using the neighbouring points $f_0(x_0, z_0)$, $f_1(x_1, z_1)$ and $f_2(x_2, z_2)$, as follows:

$$f_p(x_p, z_p) = c_a + c_x x_p + c_z z_p \tag{13}$$

where the constants come from the solution of a system of equations with three variables:

$$\begin{aligned}c_z &= \frac{(f_1 - f_0)(x_2 - x_0) - (f_2 - f_0)(x_1 - x_0)}{(z_1 - z_0)(x_2 - x_0) - (z_2 - z_0)(x_1 - x_0)}\\ c_x &= \frac{f_1 - f_0 - c_x(z_1 - z_0)}{x_1 - x_0}\\ c_a &= f_0 - c_x x_0 - c_z z_0\end{aligned} \tag{14}$$

4. RE-INITIALIZATION

The re-initialization of a level-set scalar, ϕ, to a distance function can be performed in several ways. Depending on the method, the $\phi=0$ surface may be more or less distorted by the re-initialization. One way to re-initialize is to evolve

$$\dot{\phi} = 1 - |\nabla\phi| \tag{15}$$

to steady state [8]. Another way is to use a fast marching method [9], where the algorithm builds the scalar field outward from the $\phi=0$ surface.

Because the distance function depends solely on the $\phi=0$ surface, it is essential that the solution is truly upwinding.

4.1. Re-initialization equation

The re-initialization according to Sussman *et al.* [8] is based on

$$\dot{\phi} = \mathrm{sgn}(\phi^0)(1 - |\nabla\phi|) \tag{16}$$

or

$$\phi^{n+1} = \phi^n - \Delta t\, \mathrm{sgn}(\phi^0)(|\nabla\phi| - 1) \tag{17}$$

where n is the time step number, Δt is the time step and $\mathrm{sgn}(\phi^0)$ is a sign function.

4.2. An upwind scheme for the re-initialization

If the approximation of $|\nabla\phi|$ in Equation (17) uses values from both sides of the front, $\phi = 0$, i.e. both positive and negative values, it is not upwinding because some information travels in the direction towards the front. Therefore the gradient, $|\nabla\phi|$, must be computed based on an upwinding discretization. This is accomplished by the approximation

$$\nabla\phi \approx \nabla^{\text{up}}\phi \approx \frac{\phi^n}{D} \tag{18}$$

where D is the estimated signed distance to the front, see Figure 2. D is computed from the initial field and thus preserves its value during the iterations,

$$\frac{\phi^0}{D} \approx \sqrt{\left(\frac{\Delta_x\phi^0}{\Delta x}\right)^2 + \left(\frac{\Delta_z\phi^0}{\Delta z}\right)^2} \Rightarrow D \approx \frac{\phi^0}{\sqrt{\left(\frac{\Delta_x\phi^0}{\Delta x}\right)^2 + \left(\frac{\Delta_z\phi^0}{\Delta z}\right)^2}} \tag{19}$$

The finite differences are computed as follows:

$$\begin{aligned}
\Delta_x\phi^0 &= \max\left(\frac{|\phi^0_{i+1,j} - \phi^0_{i-1,j}|}{2}, |\phi^0_{i+1,j} - \phi^0_{i,j}|, |\phi^0_{i,j} - \phi^0_{i-1,j}|, \varepsilon\right) \\
\Delta_z\phi^0 &= \max\left(\frac{|\phi^0_{i,j+1} - \phi^0_{i,j-1}|}{2}, |\phi^0_{i,j+1} - \phi^0_{i,j}|, |\phi^0_{i,j} - \phi^0_{i,j-1}|, \varepsilon\right)
\end{aligned} \tag{20}$$

Here $\varepsilon \approx 10^{-5}$, is a prescribed small number. This robust discretization is the 2D analogue of the 1D formulation in Reference [5, Equation (17)].

4.3. The smoothed sign function

The sign function, $\text{sgn}(\phi^0)$ has to be smoothed near the $\phi = 0$ surface, because the function

$$\text{sgn}(\phi^0) = \frac{\phi^0}{|\phi^0|} \tag{21}$$

is discontinuous at $\phi^0 = 0$. Instead the distance to grid ratio is used. In 1D it is written:

$$\text{sgn}(\phi^0) = \frac{D}{\Delta x} \tag{22}$$

whereas in 2D it can be written

$$\text{sgn}(\phi^0) = \frac{D}{\Delta x_e} = \frac{\phi^0}{\sqrt{\left(\frac{\Delta_x\phi^0}{\Delta x}\right)^2 + \left(\frac{\Delta_z\phi^0}{\Delta z}\right)^2}} \frac{1}{\Delta x_e} \approx \frac{\phi^0}{\sqrt{(\Delta_x\phi^0)^2 + (\Delta_z\phi^0)^2}} \tag{23}$$

The absolute value of the sign function should go to 1 when further than one grid point away from the interface. This function does this, because Δx_e is a measure of the grid size. When ϕ is not too far from being a distance function, the difference root expression is a measure of the grid size. As can be seen from Figure 3, the sign function, (21), yields 1 at $t = 1$ and

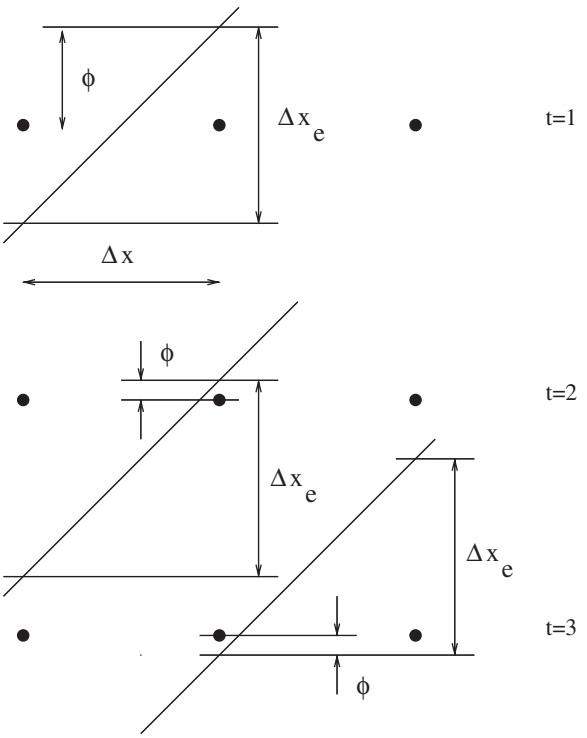

Figure 3. A level-set propagating to the right, pictured at three different times, t.

2, and -1 at $t=3$. From Equation (23) it is 0.5 at $t=1$, 0.1 at $t=2$ and -0.1 at $t=3$, i.e. this sign function is smoothed, which gives a more stable numerical solution.

4.4. The re-initialization equation with the sub-cell fix

Inserting Equations (19) and (23) in Equation (17) gives

$$\phi^{n+1} = \phi^n - \Delta t \frac{\phi^0}{\sqrt{(\Delta_x \phi^0)^2 + (\Delta_z \phi^0)^2}} \left(\left| \frac{\phi^n}{\phi^0} \right| \sqrt{\left(\frac{\Delta_x \phi^0}{\Delta x} \right)^2 + \left(\frac{\Delta_z \phi^0}{\Delta z} \right)^2} - 1 \right) \tag{24}$$

4.5. Comparison with Russo and Smereka's work

The present formulation reduces to the formulation in Reference [5] for isotropic grids. If the expression for D, Equation (19), is used together with $\Delta x = \Delta z$, then

$$D = \frac{\Delta x \phi^0}{\sqrt{(\Delta_x \phi^0)^2 + (\Delta_z \phi^0)^2}} \tag{25}$$

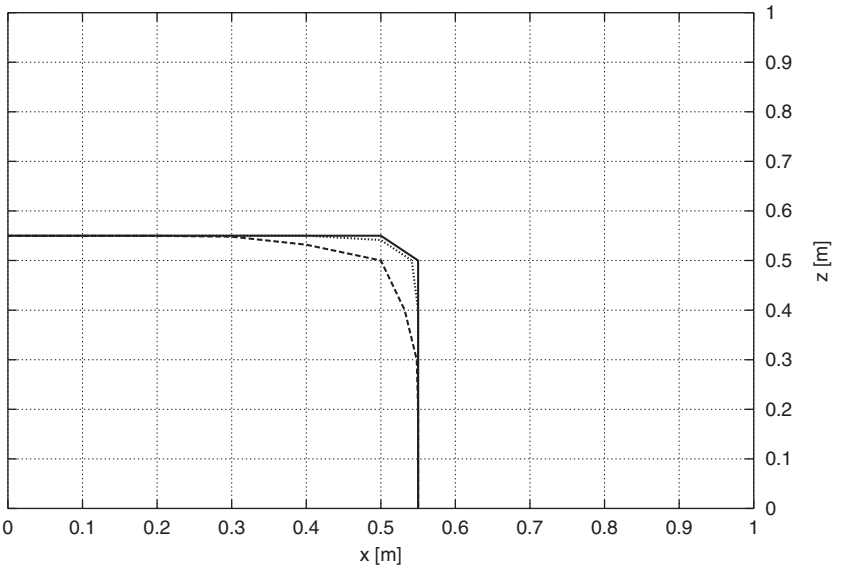

Figure 4. The $\phi = 0$ iso-contour before re-initialization (solid) and after the sub-cell-fixed (dotted) and non-sub-cell-fixed (dashed) re-initialization.

Also, on an isotropic grid, Equation (24) becomes

$$\phi^{n+1} = \phi^n - \frac{\Delta t}{\Delta x} D \left(|\phi^n| \frac{\phi^0}{|\phi^0|} \frac{1}{D} - 1 \right) \tag{26}$$

or

$$\phi^{n+1} = \phi^n - \frac{\Delta t}{\Delta x} (\mathrm{sgn}(\phi^0)|\phi^n| - D) \tag{27}$$

which is the equation for an isotropic grid of the Russo and Smereka sub-cell fix [5].

4.6. *Comparison of re-initialization methods*

The present re-initialization method with Russo and Smereka's sub-cell fix [5] is compared to the method by Sussman *et al.* [8] in Figure 4. Here, a grid of 10×10 points is used in a two-dimensional computational domain ($0 \leqslant x \leqslant 1$ m, $0 \leqslant z \leqslant 1$ m). A $\phi = 0$ surface us first prescribed. Two re-initialization methods are then applied.

As can be seen, the re-initialization without the sub-cell fix disturbs the $\phi = 0$ surface in a few grid cells around the corner. The re-initialization with the sub-cell fix also moves the surface somewhat, but this difference is negligible small.

5. PROBABILITY DISTRIBUTION OF DISTANCE FUNCTION

5.1. The test case

A two-dimensional test is designed to explore the difference between the PDF for distance function and the PDF for flame position. The test is based on the VR-1 configuration, investigated previously [3, 4]. In VR-1, a turbulent V-shaped flame is established downstream of a prismatic flame holder in a duct with a rectangular section. Only the lower half of the duct after the flame holder is considered in the present test. The flame is described with the $\bar{G}$ level-set, where $\bar{G}=0$ denotes the mean flame position. The simulated mean flame originates from the lower edge of the flame holder at $x=0$ m, $y=0.04$ m and extends through the outlet at $x=0.74$ m, $y=0.01$ m, see Figures 5 and 6. Sinusoidal waves are generated around the mean flame position ($\bar{G}=0$). The mean amplitude, amp, increases linearly along the $\bar{G}=0$ line, i.e. amp $=At$, where t is the tangential co-ordinate along the $\bar{G}$ line, see Figure 5. The amplitude and the phase of the wave are altered in such a way that the distribution of flame position along a normal, **n**, to the $\bar{G}=0$ line is Gaussian. This is accomplished by the following Box–Müller expression [10]:

$$\Upsilon = 0.5\sqrt{-2\ln(r_1)}\sin(2\pi(r_2+t)) \tag{28}$$

Here, r_1 and r_2 are independent random numbers with a uniform distribution between 0 and 1 and Υ is the position of the flame along the normal, **n**.

The wave field at one set of random numbers r_1 and r_2 is shown in Figure 6. Here the effect of re-initialization can also be seen. In the present case, the initial field is chosen to be computed with a constant ($=1$) gradient in the direction of the normal, **n**, to $\bar{G}=0$. This generates a level-set field where all levels have the same shape as the zero level. The reason for doing this is that it gives a better starting value for the re-initialization and hence speeds up the computations. The G-field is generated using:

$$G(x,y) = G_0(x,y) - \frac{At}{2}\sqrt{-2\ln(r_1)}\sin(2\pi(r_2+\mathrm{pm}\,t)) \tag{29}$$

where G_0 is the re-initialized $\bar{G}$ field around the mean line, $\bar{G}=0$, prior to the generation of the wave. A and pm are amplitude and frequency, respectively. The wavelength is related to the frequency as $wl=1/\mathrm{pm}$. The influence of A and pm can be seen in Figure 7. The factor At is proportional to the standard deviation of the flame position distribution.

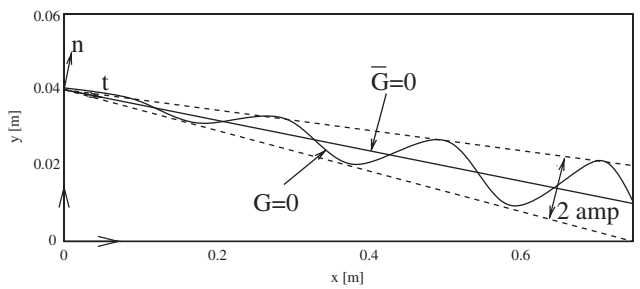

Figure 5. Sketch of a wave generated around the mean flame line, $\bar{G}=0$.

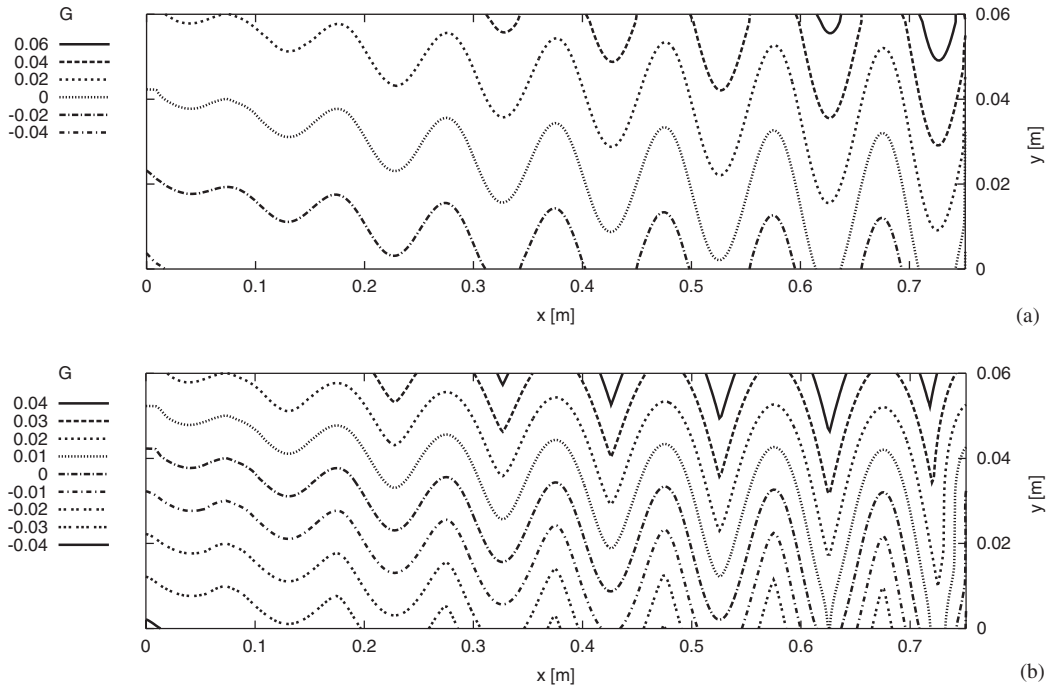

Figure 6. Initial (before re-initialization, upper figure) and re-initialized (lower figure) level-set fields of one wave realization.

Ten thousand realizations (with different r_1 and r_2) are generated and the values of G before and after re-initialization at four sampling points of the field is stored. The four points are denoted by their y-indices ($l = 2, 14, 25, 35$) and located as sketched in Figure 8. The four points are approximately located on the same normal to the $\bar{G} = 0$ line.

5.2. Grid

The grid consists of 410 times 35 nodes in x and y directions, respectively, and the cell size is $1.8\,\text{mm} \times 1.8\,\text{mm}$. The base $\bar{G} = 0$ line is computed in a real flame configuration [3, 4, 11]. The sensitivity to the grid resolution has been tested in a similar configuration with isotropic grid. For all the frequencies and all the amplitudes, except $A = 0.001\,\text{m}$, the present cell size was sufficient. The amplitude $A = 0.001\,\text{m}$ is less than the cell size, hence it is too small when using a first-order scheme.

5.3. Distributions

Figures 9, 10 and 12 show the distributions of flamelet position and the distributions of distance function for three different amplitudes, A, and the same frequency, pm. The eight diagrams in each figure show the number of hits, i.e. the number of realizations $G(x, y)$ in the incremental range $[d_A, d_B]$, where $d_B - d_A$ is the so-called bin-width. If the number of realizations goes to infinity and $d_B - d_A$ goes to zero, the number of hits divided by the

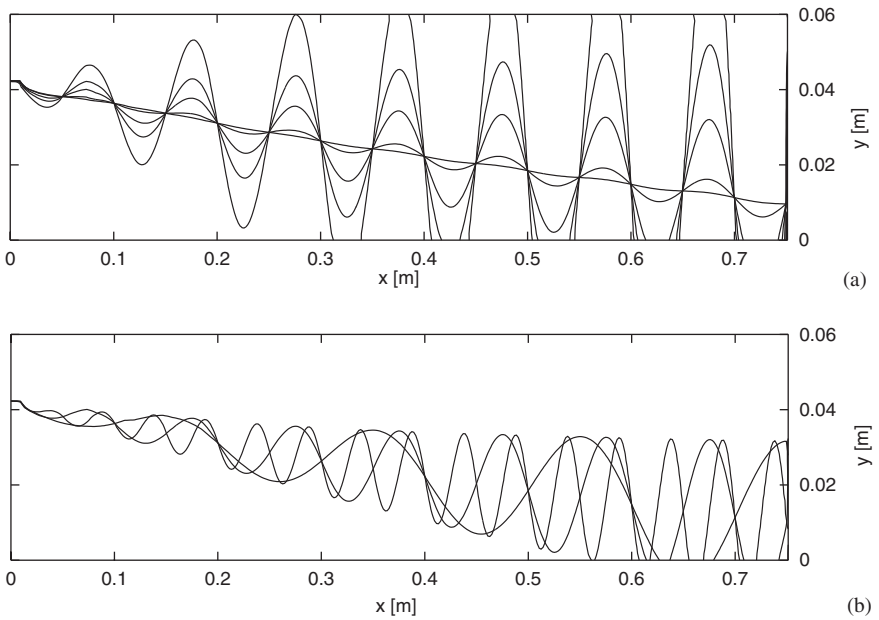

Figure 7. Waves with the same phase and period but different amplitudes (upper) and waves with the same amplitude and phase but different frequencies (lower).

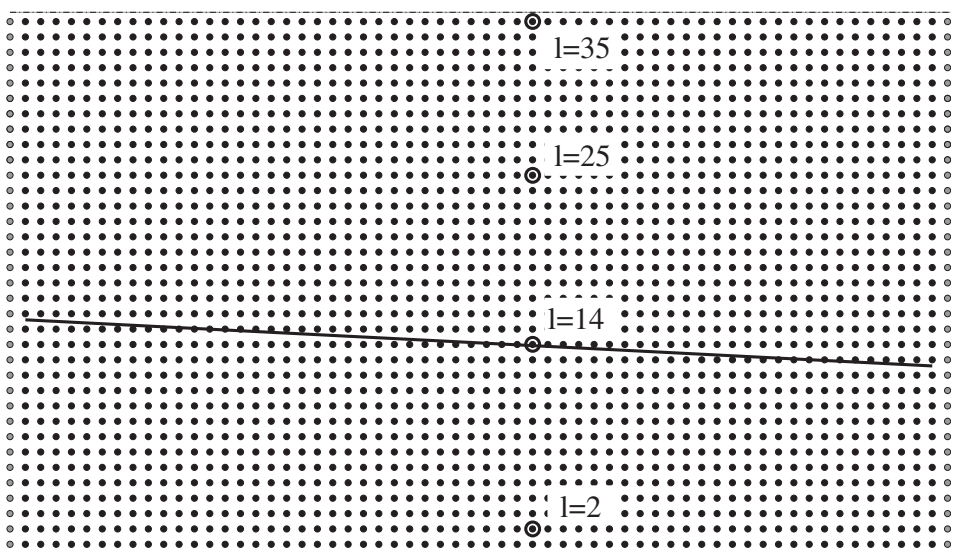

Figure 8. Sketch of the four nodes in which statistics are computed. The upper boundary is the symmetry of the duct and the lower one represents the wall. The thick line crossing the $l = 14$ node represents the $\tilde{G} = 0$ iso-contour.

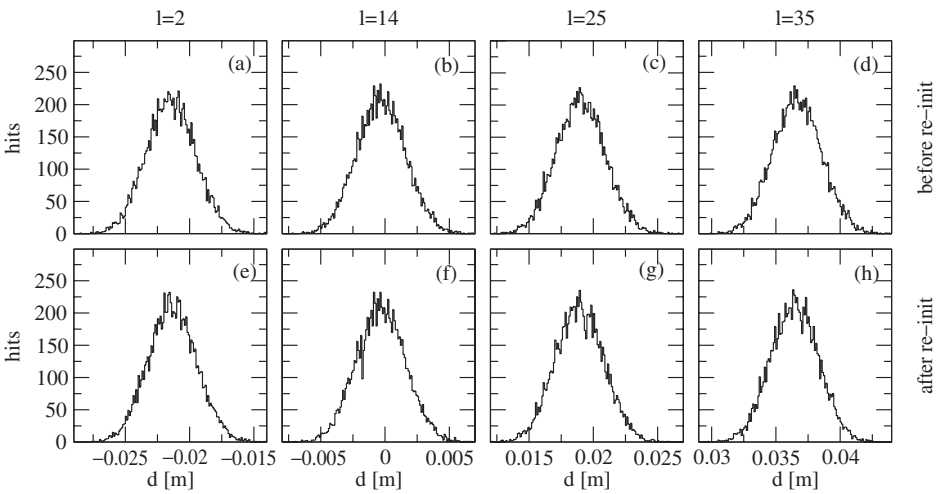

Figure 9. Distributions of flamelet position (upper) and distributions of distance function (lower) for $A = 0.01$ m and $\mathrm{pm} = 10\,\mathrm{m}^{-1}$.

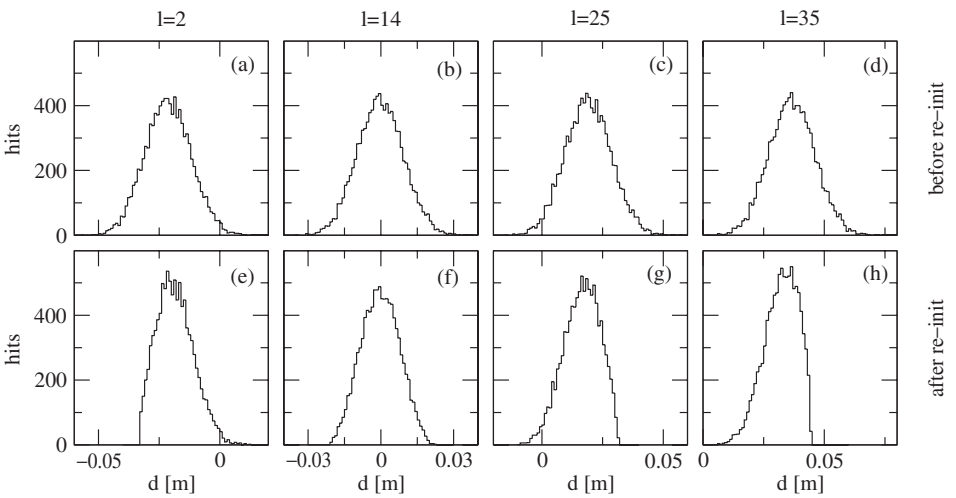

Figure 10. Distributions of flamelet position (upper) and distributions of distance function (lower) for $A = 0.05$ m and $\mathrm{pm} = 10\,\mathrm{m}^{-1}$.

number of realizations converges to a PDF. The distributions of the first rows (a)–(d) come from the wave-fields before re-initialization whereas the second row (e)–(h) presents the data after the re-initialization. Diagrams (b) represent the distribution of flamelet position around the mean flame and the diagrams of the second row (e)–(h) represent the distribution of distance function in the four sample points.

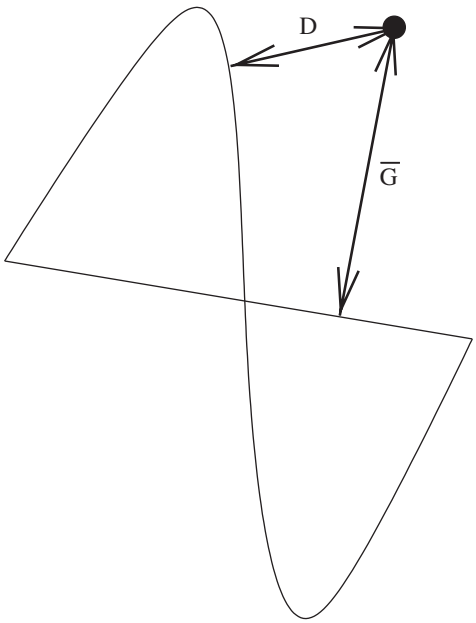

Figure 11. Sketch of an occasion when the distance function (D) is less than the distance to the mean flame surface ($\bar{G}$).

In Figure 9 the mean amplitude is very low compared to the distance from the sampling points to the mean flame. This case represents a low level of flamelet wrinkling. For such small amplitudes, the distribution is similar in all points. Here, wrinkling can be interpreted as the flame surface area to volume ratio.

In Figure 10 the wave amplitude is in the same order of magnitude as the distance from the sampling points to the mean flame. The level of flamelet wrinkling is higher. There is a clear difference between the distribution for flamelet position and the distributions of distance function. It can be seen that the distribution of distance function is skewed even at $l = 25$, which is not due to the proximity of the wall or the symmetry plane. The wall may be influential at $l = 2$ and the effect of the symmetry plane may be seen at $l = 35$. Instead, the reason is that away from the mean flame position there may always be some segment of the wave which is closer to the sampling point than the distance from the sampling point to the mean flame position (see Figure 11). An important difference, apart from the skewness, is that the mean is also different in the non-re-initialized and the re-initialized distributions. There is also a difference in the PDF shape with and without re-initialization at $l = 14$, although the mean is preserved since $\bar{G} = 0$ at $l = 14$.

In Figure 12 the level of flamelet wrinkling is very high. The mean amplitude is so high that the effects of the boundaries of the computational domain start to be evident. It can be seen even at $l = 14$ in the distribution of the re-initialized wave, the symmetry ($l = 35$) and the wall ($l = 1$) stops the distance function from being much larger than the distance limited by these boundaries. In a real V-shaped flame, there would also be interaction with the upper part of the twin flame, an effect which is neglected here.

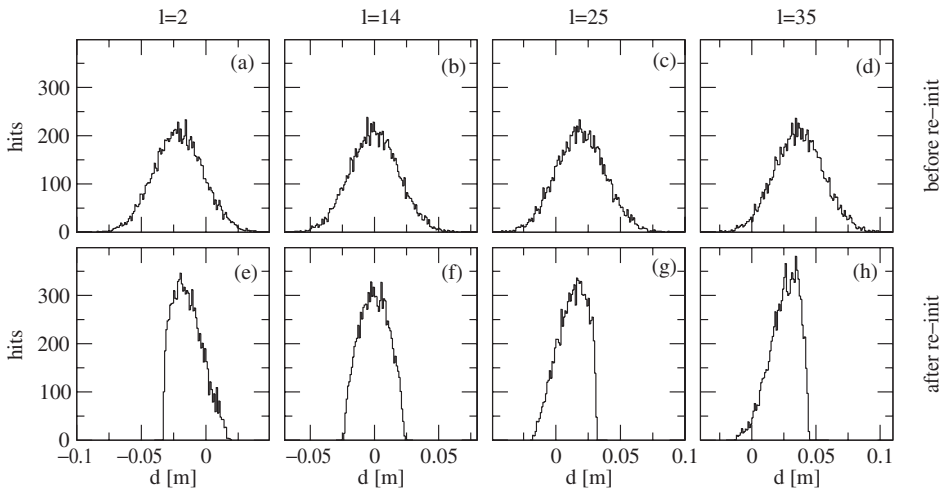

Figure 12. Distributions of flamelet position (upper) and distributions of distance function (lower) for $A = 0.1$ m and $\mathrm{pm} = 10\,\mathrm{m}^{-1}$.

5.4. Difference in distributions

A classical means for comparing probability distributions is the Kolmogorov–Smirnov test. Here, a two-sample version of this test is employed to compare the corresponding distributions from the sample points $l = 2$, 25 and 35 with the distribution from $l = 14$. The test is performed using the mathematical software Octave and the function therein.

In short it works as follows. The N independent samples are $x_0 \ldots x_{N-1}$. $S(x_j)$ is the fraction of observations less than or equal to x_j. $F(x)$ is the reference cumulative distribution, which in this two-sample test is the cumulative distribution at $l = 14$. The Kolmogorov–Smirnov test statistic is computed by

$$ks = \sqrt{N} * \max(|S(x_j) - F(x_j)|) \tag{30}$$

The test statistic is usually compared to tabulated critical values in order to determine at which level of confidence the distribution $S(x)$ is the same as $F(x)$. The lower the value, the higher the probability that the distributions are the same. Here the interest is, however, more in the relative values and no comparison to the critical is made. The results of the test are shown in Figure 13. As expected, increasing wave amplitude leads to increasing the difference between the distributions. At the lowest values of A, the influence of the grid resolution starts to be influential. Here A is of the same order as the resolution. It is also rather clear how the distance from the sample point to the $l = 14$ point affects the solution, because the difference in $l = 2$ and 25 which are at a similar distance from $l = 14$ typically gives the same difference, which is lower than the difference at $l = 35$. Increasing the wave frequency, pm, also increases the difference.

5.5. Detailed investigation of PDFs

In order to investigate the difference between the PDF of flame position and the PDF of distance function at different positions inside and outside the flame brush in more detail, a

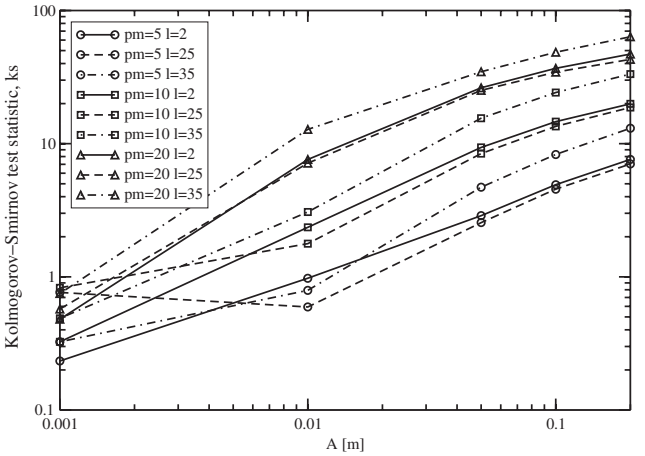

Figure 13. Two-sample Kolmogorov–Smirnov test comparing the distribution at $l = 2$, 25 and 35 to the corresponding distribution at $l = 14$. The grid size is $\Delta x = 0.0018$ m.

rectangular test box is devised. The test box is 1 m wide (x direction) and 2 m high (y direction). The $G = 0$ surface, which is modelled here by sine waves according to Equation (29), is given at a quarter of the height ($y = 0$, see Figure 14). The wavelength is set to twice the amplitude and again 10 000 realizations with different r_1 and r_2 are generated. This figure also shows the re-initialized G-field for the realization. In this configuration, co-ordinate y represents the distance to the mean flame position.

In a real flame, the eddies wrinkle the flame so that the wavelength is roughly some multiple of the amplitude, see Figure 15. However, a real flame is affected by a spectrum of eddy sizes whereas the present test flame is only affected by one size at a time. Nevertheless, the influence of the flamelet wrinkling on the PDF of distance function is qualitatively retained in this test.

The grid consists of 50×100 mesh points in x and y directions, respectively. The resulting statistics are computed with the Octave software and presented in Figure 16.

The mean distance function represents the mean value of the distance to the instantaneous laminar flamelet. It is shown to be fairly different from the distance to the mean flame (co-ordinate y in Figure 16). The mean value of the distance function is a linear function of y at points far away from the mean flame position ($y > 0.3$ m). Around the mean flame position, the mean value of the distance function varies very slowly with respect to y, the distance to the mean position (the curves for the mean have a zero gradient at $y = 0$). This flattening is more pronounced for wavelengths which are short compared to the amplitude, i.e. for highly wrinkled flames. As a summary, we notice that

$$\begin{aligned} &|\nabla \bar{G}| = 1 \text{ far away from the mean flame brush} \\ &|\nabla \bar{G}| \ll 1 \text{ inside the mean flame brush} \end{aligned} \tag{31}$$

This result is important for the RANS FLA. It implies that in the re-initialization equation (Equation (2)), variable σ is fairly different in different regions of the flowfield. Special care

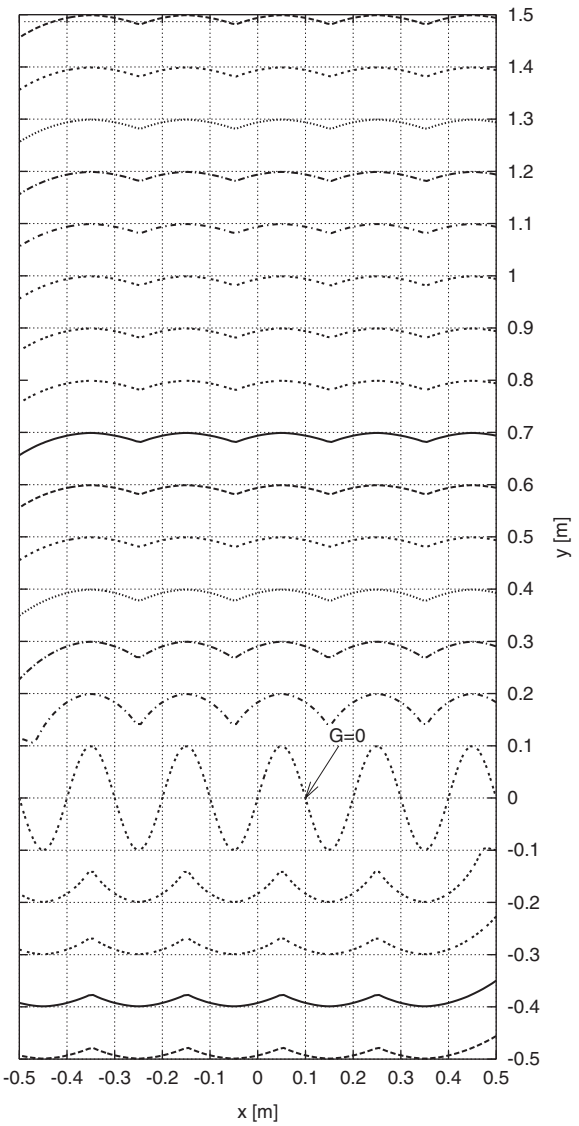

Figure 14. Computational domain for testing details of the PDF for distance function. One realization of flame position ($G = 0$) and the re-initialized G-field are shown.

has to be taken in the re-initialization. Peters [2] proposed a co-ordinate stretching method: Equation (2) with $\sigma = 1$ is first solved; the calculated $\tilde{G}$ field is then re-scaled by the factor σ which is modelled as the ratio of wrinkled flamelet surface area to the mean flame surface area. Since $\sigma \gg 1$, the condition $|\nabla \tilde{G}| \ll 1$ is fulfilled. In a recent work [4], it was shown that the re-scaling of distance function can lead to significant improvement of the simulation of intermediate species. As noted, the co-ordinate stretching method is not valid for the flowfield

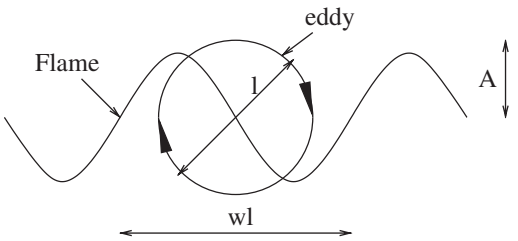

Figure 15. Sketch of an eddy wrinkling the flame.

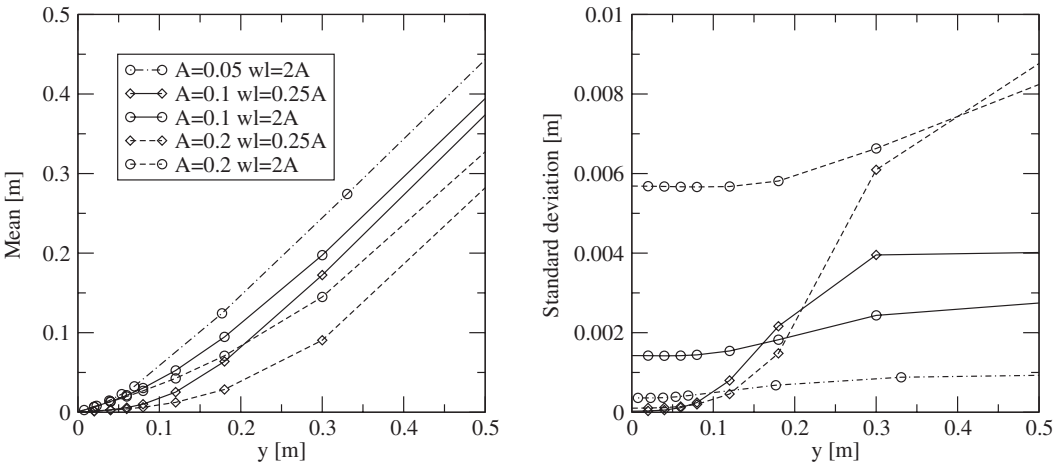

Figure 16. Simulated mean and standard deviation of the distance function for different wavelength and amplitude.

far away from the mean flame brush. A more accurate model for the re-initialization of the mean distance function is needed.

The standard deviation of the distance function may be approximated as constant along the normal to the mean flame surface, as shown by the standard deviation as a function of y being rather flat when the wavelength is a multiple of the amplitude (lines with circle symbols). This is particularly true in the mean turbulent flame brush. The value of the standard deviation of distance function is closely related to the standard deviation of the flamelet position (which is proportional to the wave amplitude here).

5.6. *Application to flame simulation*

The above simulated sine wave flame may be used directly in the prediction of a premixed turbulent flame together with a flamelet library (using Equation (3)). Figure 17 shows the CO mole fraction obtained with two different methods: the D-PDF and the P-PDF methods. In the D-PDF method, the instantaneous distance function at $G \neq 0$ is calculated after each realization of the instantaneous flame surface ($G = 0$). Therefore, the effect of flame wrinkling

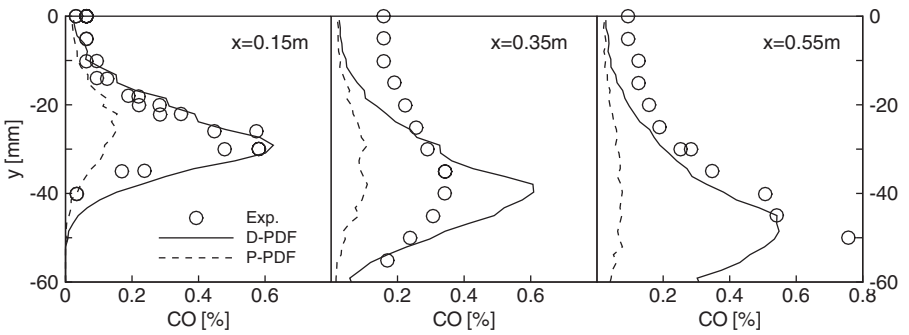

Figure 17. CO mole fraction from a previous experiment [11] and from numerical simulations using two different PDF approaches.

on the skewness and shape of the distance function PDF is taken into account. In the P-PDF approach, the shape of PDF of the distance function is assumed to be the same as that of the flamelet position (here a Gaussian distribution is assumed), and the mean distance function is calculated using Equation (2) with $\sigma = 1$. Here the amplitude and frequency are set to $\text{amp} = 0.04t + 0.01\,\text{m}$ and $\text{pm} = 250\,\text{m}^{-1}$. $t = \sqrt{x^2 + (y + 0.04)^2} \approx x$. As can be seen from Figure 17, the predictions improve significantly when the effect of flamelet wrinkling on the PDF of the distance function is taken into account (D-PDF). When the PDF of distance function is assumed to be the same as the one of the flamelet position (P-PDF), the simulated CO is much lower than the measurement. More details about the experimental data can be found in Reference [11]. The reason for this is the increased probability of being close to a flamelet in the mean flame brush. This is particularly important for intermediate species, which only exist in a thin layer in the flamelet co-ordinate [4].

The integrated sinus wave arc length per unit length of mean flame line varies from 12 at the flame holder to 32 at the outlet. This is comparable to the ratio of the wrinkled flame surface area to the mean surface area, which in the present case is about 10. As seen, they are in the same order of magnitude. The prediction can be improved when a more realistic shape of flamelet wrinkling (a three-dimensional fractal surface) is considered.

6. CONCLUDING REMARKS

The difference between the probability distribution of flamelet position and the distribution of distance function has been investigated. It is shown that the distribution of distance function is skewed at positions away from the mean flame surface, particularly at distances comparable to the amplitude.

- The mean distance function is not equivalent to the distance to the mean flame position, i.e.

$$|\nabla \bar{G}| \neq 1 \tag{32}$$

which has been argued previously [2]. Around the mean flame position ($\bar{G} = 0$), the mean distance function varies very slowly. Outside the flame brush, the mean distance function is a linear function of the distance to the mean flame position.

- The standard deviation of the distance function can be approximated as constant when the flame wrinkling amplitude is comparable to the wrinkling wavelength, i.e.

$$\nabla\sigma \cdot \nabla\bar{G} \approx 0$$

An extension method for the solution of this equation is presented.

- Close to the mean flame position ($|\bar{G}| \sim \text{amp}$), the shape of the distance function PDF may be presumed to be similar to the flame position PDF, if amp is small compared to the combustor size.

The present sinusoidal shape does not resemble a real flame structure exactly. A real flame structure has a fractal shape with a whole spectrum of wrinkling amplitudes and wavelengths overlayed. In a continuation of this work, a more realistic flame shape may be used, perhaps also in three dimension. It may be interesting to study the distributions of other flame properties, e.g. of inclination relatively the mean flame surface and of flame surface density.

A model based on the distributions of distance to flamelet, obtained by Monte-Carlo simulations from presumed distributions of flame position and inclination may be developed.

ACKNOWLEDGEMENTS

This work was supported by the Swedish National Energy Administration's Consortium for Gas Turbine Centre (GTC) and the Swedish Research Council (VR).

REFERENCES

1. Williams FA. Turbulent combustion. In *The Mathematics of Combustion*, Buckmaster J (ed.). SIAM: Philadelphia, PA, 1985; 97–131.
2. Peters N. *Turbulent Combustion*. Cambridge University Press: Cambridge, 2000.
3. Nilsson P, Bai XS. Level-set flamelet library approach for premixed turbulent combustion. *Experimental Thermal and Fluid Science* 2000; **21**:87–98.
4. Nilsson P, Bai XS. Effects of flame stretch and wrinkling on CO formation in turbulent premixed combustion. *Proceedings of the Combustion Institute*, vol. 29, 2003, at press.
5. Russo G, Smereka P. A remark on computing distance functions. *Journal of Computational Physics* 2000; **163**:51–67.
6. Sheperd IG, Hubbard GL, Talbot L. The dynamic structure of turbulent V-shaped premixed flames. *Proceedings of the Combustion Institute* 1986; **21**:1377–1383.
7. Chen Y-C, Peters N, Schneemann GA, Wruck N, Renz U, Mansour MS. The detailed flame structure of highly stretched turbulent premixed methane-air flames. *Combustion and Flame* 1996; **107**:223–244.
8. Sussman M, Smereka P, Osher S. A level set approach for computing solutions to incompressible two-phase flow. *Journal of Computational Physics* 1994; **114**:146–159.
9. Sethian JA. *Level set methods and fast marching methods*. (2nd edn). Cambridge University Press: Cambridge, Cambridge Monographs on Applied and Computational Mathematics, 1999.
10. Box GEP, Müller ME. A note on the generation of random normal deviates. *Annals of Mathematical Statistics* 1958; **29**:610–611.
11. Sjunnesson A, Olovsson S, Sjöblom B. Validation rig—a tool for flame studies. In *Volvo Flygmotor Internal Report*, VFA 9370-308, 1991.

